Performance Analysis of a Perovskite-Based Thing-to-Thing Optical Wireless Power Transfer System

Dinh Hoa Nguyen, *Member, IEEE*, Ganbaatar Tumen-Ulzii, Toshinori Matsushima, and Chihaya Adachi

***Abstract*—This paper presents an analysis on the performance of an optical wireless power transfer system in which optical transceivers made from a perovskite are used. Experiments are performed under different settings, whose resulted data reveal interesting findings. First, system performance is only matched with the existing theory when no collimating lens is employed. Hence, a data-driven mathematical model is proposed and verified when a collimating lens is used. Second, a collimating lens helps increase the amount of wirelessly transferred power and the transfer distance if perfect alignment between optical transceivers is guaranteed, but substantially limits the sliding distance between them otherwise.**

***Index Terms*—Bidirectional wireless power transfer, data-driven mathematical modeling, optical transceiver, optical wireless power transfer, perovskite light-emitting diodes, perovskite solar cells.**

I. Introduction

OPTICAL wireless power transfer (OWPT) is an emerging and promising approach applicable in many practical systems including internet of things [1], [2], consumer electronics [1], [3], implantable medical devices [4]–[6], vehicle electrification [7]–[12], robotics [7]–[12], etc. OWPT systems possess unique features that other WPT systems do not have. First, OWPT systems are capable of harvesting ambient light energy in the absence of optical transmitters, for instance, from sunlight and indoor lighting equipment. Therefore, OWPT systems can be self-charged even when the primary side, i.e., the optical transmitters, are not present, which is extremely important and convenient for numerous applications such as implant medical devices and biosensors, wearable electronics, etc. Second, OWPT systems have relatively simple electronic circuits and can be flexibly attached on uneven surfaces [7]. Third, OWPT systems have the capability of simultaneous information and power transfer [13]. Last but not least, OWPT systems can be utilized in different environments, namely air, water, space, under the skin [7], [14], in brain science [15], [16], and even at the nanoscale [17].

In our previous study [7], we proposed a thing-to-thing OWPT (T2T-OWPT) network in which hybrid perovskite solar cells serve as optical transceivers capable of both emitting and absorbing light. The advantages obtained when using optical transceivers are on the potentials of simpler structure, lighter weight, lower cost, and better functionality, flexibility, and convenience for the OWPT system [7]. For instance, any device equipped with our proposed perovskite optical transceiver can be self-charged when it is not in the light-emitting mode, which was not possible in conventional OWPT systems where optical transmitting devices cannot work in light absorption mode. Initial experimental results were reported in [7] for our perovskite cells working in both light emission and absorption modes, which proved the feasibility of our proposed T2T-OWPT concept. However, no results have been reported so far when our proposed T2T-OWPT system operates in different conditions which are close to realistic situations, for example, when the optical transceivers are not properly aligned.

On the other hand, there have been a few studies in the literature to examine the operation of OWPT systems under changing conditions. In [18], simple formulas were used to calculate the OWPT system efficiency when the solar cell attached on the optical receiver was partially covered by the light beam from the laser transmitter. Moreover, when a reflection mirror was used to improve the efficiency, no mathematical analysis was provided in [18]. Next, the research in [19] proposed and analyzed simultaneous mobile information and power transfer system, where the laser emitter was fixed while the optical receiver could be moving. A mathematical model was then proposed in [19] for the mobile optical coupling link.

In the current work, we present our latest results on the operation of our proposed T2T-OWPT concept as well as the related theoretical and empirical analyses. More specifically, we perform different experiments on the OWPT between two identical perovskite solar cells under different settings including perfect and imperfect alignment that are likely happened in realistic situations, and in the presence and absence of a collimating lens. Obtained experimental results are then analyzed and compared with the existing theory. Remarkably, when no collimating lens is employed, our experimental results are matched with that from the existing theory. Nevertheless, it is

Manuscript received November 30, 2021; revised January 11, 2022; accepted January 21, 2022. Date of publication January 27, 2022; date of current version February 7, 2022. This work was supported in part by the JSPS KAKENHI under Grants JP19K15013 and JP20H02817, in part by the Samco Foundation, in part by the Iketani Science and Technology Foundation, in part by the Murata Science Foundation, and in part by the Iwatani Naoji Foundation. (*Corresponding author: Dinh Hoa Nguyen.*)

The authors are with the International Institute for Carbon-Neutral Energy Research (WPI-I^{2}CNER), Kyushu University, Fukuoka 819-0395, Japan (e-mail: hoa.nd@i2cner.kyushu-u.ac.jp; ganbaatartu@i2cner.kyushu-u.ac.jp; tmatusim@i2cner.kyushu-u.ac.jp; adachi@cstf.kyushu-u.ac.jp).

Digital Object Identifier 10.1109/JPHOT.2022.3146365

interesting that when a collimating lens is used, the obtained experimental results are completely different that cannot be explained with the existing theory. As such, we empirically propose a mathematical model to capture the essence of those experimental results. Our proposed data-driven mathematical model, therefore, contributes a useful result to the literature that would facilitate further understandings, in particular when the T2T-OWPT systems are implemented in realistic situations, and for OWPT systems in general.

The remainder of this paper is organized as follows. The performance of perovskite-based devices operating in the light emission and absorption modes is presented in Section II. Theoretical results on the optical transmission are revisited in Section III. Experimental results on the OWPT between perovskite transceivers without any lens are given and analyzed in Section IV. Then experimental data on the OWPT between perovskite transceivers with a collimating lens are introduced in Section V, showing that they are not fitted into the theory introduced in Section III. To explain the experimental results in Section V, a data-driven mathematical model is proposed and validated in Section VI. Finally, a summary of the main results in this study and directions for the future research are provided in Section VII.

II. Performance of Perovskite-Based Devices

The perovskite-based device architecture is glass substrate/indium tin oxide anode layer (∼100 nm)/tin oxide electron transport layer (∼30 nm)/perovskite layer (∼650 nm)/*N*,*N*-di(4-methoxy-phenyl)amino]-9,90-spirobifluorene (spiro-OMeTAD) hole transport layer (∼150 nm)/gold electrode (∼80 nm), which is a widely used architecture in the research field of perovskite solar cells. We used the large perovskite layer thickness of ∼650 nm to efficiently absorb the light coming from other perovskite device operating in the light emission mode. The composition of the perovskite layer was $Cs_{0.05}(FA_{0.85}MA_{0.15})_{0.95}Pb(I_{0.85}Br_{0.15})_3$. Here, FA is the formamidinium and MA is the methylammonium. The spiro-OMeTAD layer was doped with lithium bis(trifluoromethanesulfonyl)imide (Li-TFSI), tris(2-(1H-pyrazol-1-yl)-4-tert-butylpyridine)cobalt(III)tri[bis(tri-fluoromethane)sulfonimide] (FK-209), and 4-tert-butylpyridine (4-tBP) to increase the electrical conductivity and device performance. Please see [20], [21] for the device fabrication and evaluation. Under the simulated solar illumination (100 mW/cm^2 and AM1.5G), the current density−voltage curve of perovskite-based devices was measured and depicted in Fig. 1(a). By analyzing this curve, a short-circuit current density of ∼23.8 mA/cm^2, an open-circuit voltage of ∼1.17 V, a fill factor of ∼0.73, a series resistance of $\sim 1.88 \times 10^2\ \Omega$, and a shunt resistance of $2.17 \times 10^6\ \Omega$ were obtained. Then multiplying the short-circuit current density, open-circuit voltage, and fill factor gives us a power conversion efficiency (PCE) at ∼20.2%. Next, when we applied an external voltage to the same devices, the perovskite cells started to show electroluminescence. The maximum external quantum efficiency (electron-to-photon conversion) was ∼1.5%, as shown in Fig. 1(b).

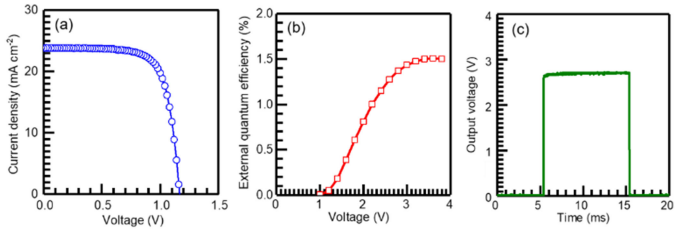

Fig. 1. (a) Current density−voltage curve of perovskite-based devices operating in the light absorption mode under the simulated solar illumination. (b) External quantum efficiency−voltage curve of perovskite-based devices operating in the light emission mode. (c) One example of the output signal wave obtained by optical wireless transmittance between two perovskite devices.

The aforementioned results clearly indicate that our perovskite-based devices not only can be operated in both the light absorption and emission modes but also have been improved to have higher performances compared to the perovskite cells previously introduced in [7]. The electroluminescence peak wavelength was ∼790 nm, at which the light absorption band of the perovskite exists. In other words, the emission band overlaps with the absorption band. By employing this self-absorption effect, the OWPT system construction is possible by emitting the photons from one-side perovskite device operating in the light emission mode and then absorbing the photons by the other perovskite device operating in the light absorption mode. Please refer to [7] for the operation concept of our OWPT system using the two perovskite devices and discussion on its system efficiency.

Perovskite light-emitting diodes (PeLEDs) are known to be very unstable under continuous operation. Although many researchers are now investigating the degradation mechanisms of PeLEDs for better operational durability [22]–[24], our perovskite-based devices operating in the light emission mode were very unstable as well. Electroluminescence intensity quickly degraded within one hour even under the operation at a low current density level such as 1 mA/cm^2. We need a further study to improve the operational durability of PeLEDs. To avoid the degradation during the optical transmission experiments, a perovskite device was driven to generate electroluminescence under electrical pulse excitation. For this, a multifunction generator (WF1973, NF) was used. The voltage was 8 V, the pulse width (ON time) was 10 ms, and the OFF time was 190 ms. The electroluminescence from the pulse-driven perovskite device was detected by the other perovskite device of the same architecture. This perovskite device operating in the light absorption mode was connected with a 50 Ω resister. With this low resistance, the operating condition of the device is close to the short circuit. The voltage signals, which were converted from the current signals coming from the device and amplified by ∼100 times using a low-noise amplifier (T-01LNA, Turtle Industry Co.) and averaged over hundreds of the measurements to improve a signal-to-noise ratio, were detected with an oscilloscope (DS-5105B, Iwatsu). The voltage signals displayed on the oscilloscope looked a nearly square wave shape as shown in Fig. 1(c) and were very stable, without a decrease in signal intensity, pointing to the negligible degradation during

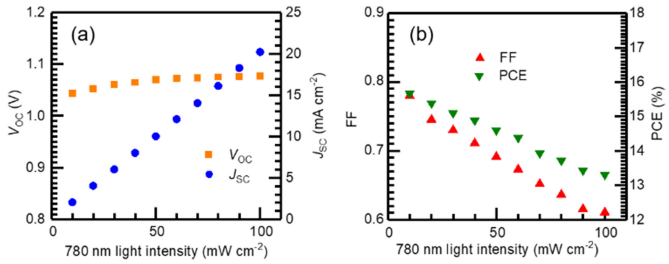

Fig. 2. Light intensity-dependent characteristics of our perovskite solar cells. (a) V_{OC} and J_{SC}. (b) FF and PCE.

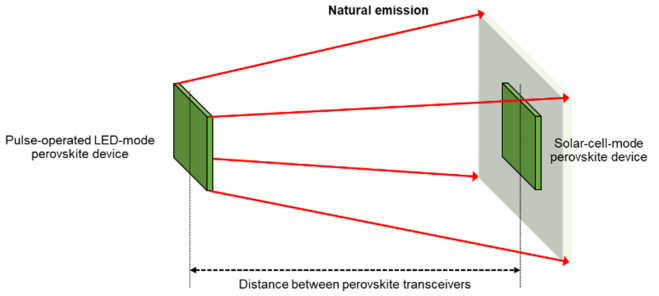

Fig. 3. System setup in Scenario 1.

the measurements. The values used on the vertical axis of the experimental plots discussed later mean the obtained output signals.

Next, we measured light intensity-dependent current density−voltage curves of our perovskite solar cells. As a light source, we used a commercial 780 nm LED. This light wavelength is close to the EL peak wavelength measured from the same device architecture operating in the light emission mode (∼790 nm). As can be seen in Fig. 2(a) and (b), the open-circuit voltage V_{OC} is increased and the fill factor FF is decreased as the light intensity is increased. The light intensity-dependent V_{OC} is normally seen in solar cells, with slopes in between kT/q and $2kT/q$ which indicate the bimolecular and trap-assisted recombination, respectively [25]–[27], where k is the Boltzmann's constant, T is the temperature, and q is the charge of an electron. The slope of our V_{OC} in a linear–logarithmic scale is $1.36kT/q$, which means that both the bimolecular and trap-assisted recombination exit in our solar cells. However, the decrease in FF at the higher light intensity indicates that the bimolecular recombination is more dominant than the trap-assisted recombination since the bimolecular recombination rate is proportional to the photogenerated charge carrier density [25]–[27]. Because of the aforementioned decrease in FF, the overall PCE is decreased as the light intensity is increased, as observed in Fig. 2(b). Finally, the short-circuit current J_{SC} is linearly increased with the increase of the light intensity, with a correlation coefficient R of 0.99992 (see Fig. 2(a)). Therefore, the solar cell output plots presented in the next sections do not include the non-linearity effect of the device performance. Moreover, this linearity of J_{SC} implies that we can estimate the output of our perovskite transceiver when it is illuminated with the superposition of multiple perovskite transceivers, by summing up its outputs as being individually illuminated by each of those perovskite transceivers. Thus, in what follows we consider the OWPT between two identical perovskite transceivers, one works in the light emitting mode and the other works in the light absorbing mode.

III. Theoretical Analysis of OWPT Using Perovskite Transceivers

The following mathematical formula has been widely used to calculate the DC optical gain of optical links from LEDs, and has also been employed in OWPT systems [7], [8],

$$H(0) = \begin{cases} \frac{(m_l+1)A}{2\pi d^2}\cos^{m_l}\phi g_f(\varphi)\, g_c(\varphi)\cos\varphi : 0 \le \varphi \le \varphi_w \\ 0 : \ \varphi > \varphi_w \end{cases} \tag{1}$$

in which A is the physical area of the optical receiver, d is the optical transmission distance, φ is the angle of incidence (i.e., the angle at which the receiver sees the transmitter), ϕ is the angle of irradiance (i.e., the angle at which the transmitter sees the receiver), $g_f(\varphi)$ is the gain of an optical filter, $g_c(\varphi)$ is the gain of an optical concentrator, and φ_w is the width of the field of view (FOV) at the optical receiver. If no optical filter and concentrator are used, then their gains are omitted in (1). Moreover, m_l denotes the order of Lambertian emission which is given by the semi-angle at half illuminance $\phi_{1/2}$ of an LED as follows,

$$m_l = -\frac{\ln 2}{\ln\left(\cos\Phi_{1/2}\right)}$$

In the context of OWPT systems, $\cos\phi = 1$ and $\cos\varphi = 1$ in (1) when two perovskite transceivers are perfectly aligned (see Fig. 3). This means theoretically the optical link DC gain in our considering perovskite-based OWPT systems is inversely quadratically dependent on the distance between the perovskite transceivers. Nevertheless, when two perovskite transceivers are not perfectly aligned, $\cos\phi$ and $\cos\varphi$ will be variant. As such, the optical link DC gain in the considering OWPT systems would no longer be a quadratic function of the inverse of the distance between the transmitter and the receiver. In the next section, we will perform different experiments to verify this theoretical formula and accordingly propose a new data-driven mathematical model for the results that do not fit into it.

IV. Experiment on Perovskite-Based OWPT Without Lens

This section is devoted to analyze the performance of a perovskite-based T2T-OWPT system in which no lens is used. Different tests are performed under which the perovskite optical transmitter and receiver are perfectly and imperfectly aligned. It turns out that experimental data are well-matched with the theory presented in Section III, i.e., they follow the rule set in (1). Details on those tests are provided below.

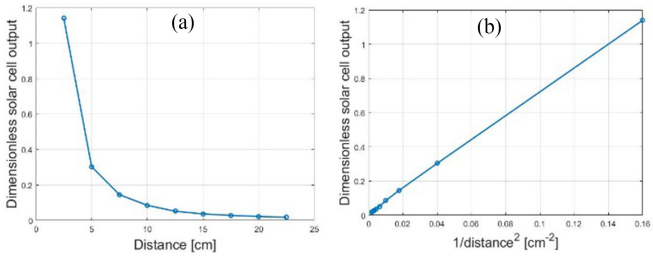

Fig. 4. System output versus optical wireless power transfer distance, when no lens is used.

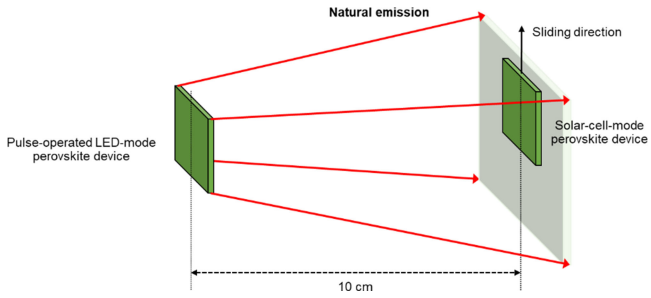

Fig. 5. System setup in Scenario 2.

A. Scenario 1: Perovskite Optical Transceivers are Precisely Aligned

In this scenario, two perovskite transceivers are arranged in parallel and aligned perfectly. No lens is utilized, hence the light beam from the perovskite optical transmitter is spread. The system setup is demonstrated in Fig. 3.

Experimental results for Scenario 1 are depicted in Fig. 4. As seen from Fig. 4(b), the output of the perovskite optical receiver is almost inversely linearly decreased with respect to the square of the distance between two perovskite transceivers. This coincides with the theoretical analysis introduced in Section III.

B. Scenario 2: Perovskite Optical Transceivers are Vertically Slid

This experiment examines the system operation when two perovskite optical transceivers are not perfectly aligned, which likely happens in realistic situations. Particularly, we fix the perovskite optical transmitter while sliding the perovskite optical receiver vertically to observe how the receiver output varies. The distance between the two device planes containing perovskite optical transceivers is kept constant at 10 cm, as depicted in Fig. 5.

In this case, the angle of incidence φ and the angle of irradiance ϕ are equal and dependent on the sliding distance. Taking the natural log on both sides of (1) results in the following linear relationship between the log of the optical link DC gain and the log of $\cos\varphi$, when the angle of incidence is not larger than the width of the FOV at the optical receiver.

$$\log\left(H\left(0\right)\right) = \left(m_l + 1\right)\log\left(\cos\varphi\right) + \log\left(\frac{\left(m_l + 1\right)A}{2\pi d^2} g_f\left(\varphi\right) g_c\left(\varphi\right)\right) \quad (2)$$

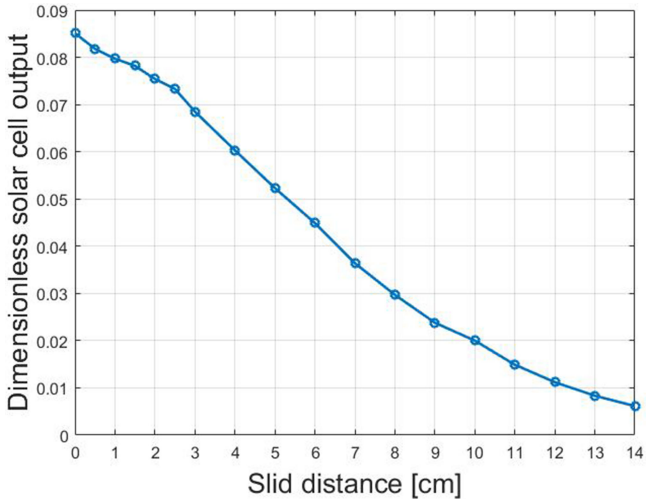

Fig. 6. System output versus slid distance between the optical transmitter and receiver, when no lens is used.

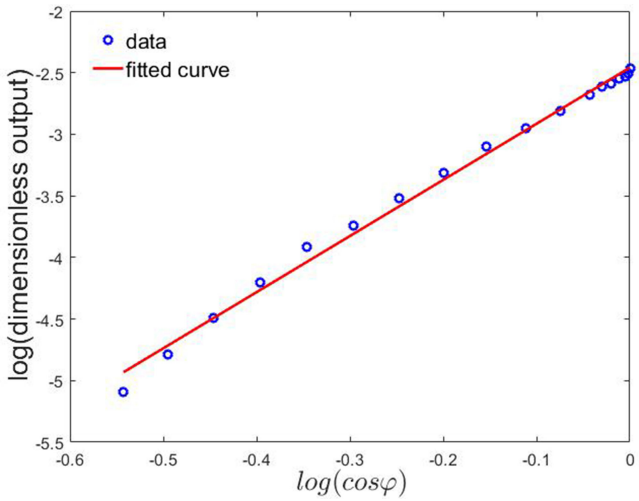

Fig. 7. Verification of experimental data to theoretical result in Scenario 2.

Experimental results for Scenario 2 are exhibited in Fig. 6. Obviously, without a collimating lens, the light beam from the perovskite optical transmitter is spread, which helps increase the success of wirelessly transmitted power to the optical receiver. As a result, the wireless power transfer can be sustained at a long slid distance. Moreover, the output of the perovskite optical receiver is reduced slowly. Next, we compare the experimental data with the theoretical formula in (2). Results plotted in Fig. 7 show that the log of the perovskite optical receiver output is closely to be linearly dependent on the log of $\cos\varphi$, i.e., (2) is almost held in this scenario.

C. Scenario 3: Perovskite Optical Transceivers are Rotated

In this scenario, the system operation is examined when two perovskite optical transceivers are also not perfectly aligned, but unlike that in Scenarios 1 and 2, the situation we are considering here is when one perovskite cell is rotated with respect to the other. In particular, let us fix the perovskite optical

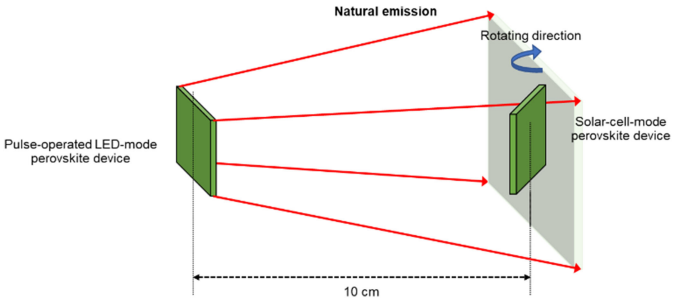

Fig. 8. System setup in Scenario 3.

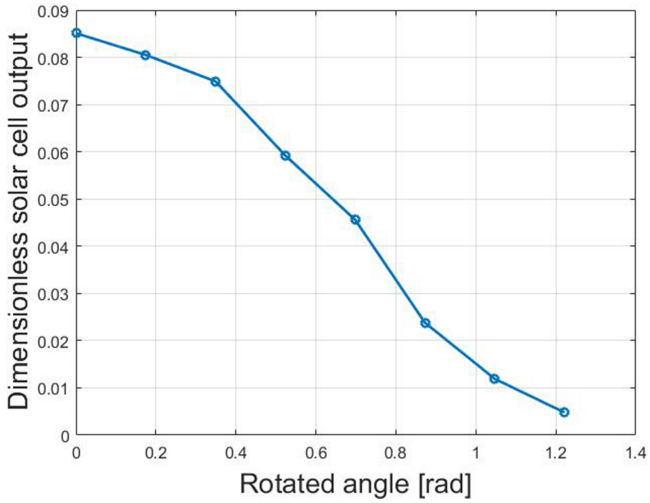

Fig. 9. Verification of experimental data to theoretical result in Scenario 3.

transmitter whilst rotating the perovskite optical receiver, as shown in Fig. 8. The distance between the centers of perovskite optical transceivers is also kept constant at 10 cm. We can verify similarly the system operation when one perovskite cell is rotated in another direction, hence we do not present here for brevity.

In this scenario, the angle of irradiance $\phi = 0$, while the angle of incidence φ is equal to the rotating angle. Subsequently, taking the natural log on both sides of (1) gives us the following linear relationship between the log of the optical link DC gain and the log of $\cos\varphi$, when the angle of incidence is not larger than the width of the FOV at the optical receiver.

$$\log\left(H\left(0\right)\right) = \log\left(\cos\varphi\right) + \log\left(\frac{\left(m_l+1\right)A}{2\pi d^2} g_f\left(\varphi\right) g_c\left(\varphi\right)\right) \tag{3}$$

Experimental results for Scenario 3 are plotted in Fig. 9. Next, Fig. 10 shows the relation between the log of the perovskite optical receiver output and the log of $\cos\varphi$. It can be seen from Fig. 10 that the above-mentioned relation is almost linear with obtained experimental data, hence validating (3).

V. Experiments on Perovskite-Based OWPT With a Collimating Lens

This section presents our experimental results on the same system setups as that in Section III, except that a collimating

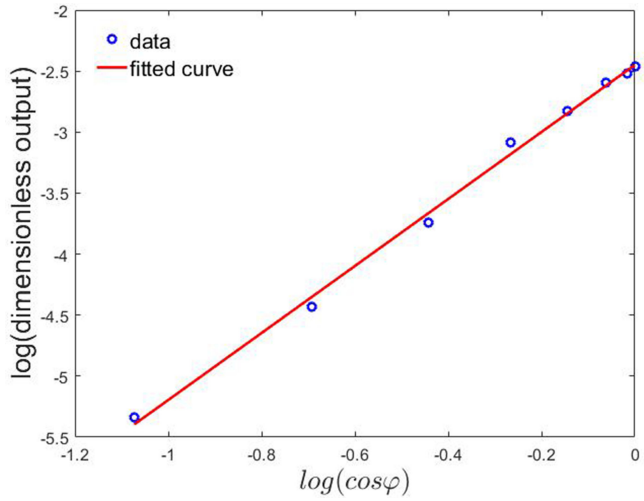

Fig. 10. Verification of experimental data to theoretical result in Scenario 3.

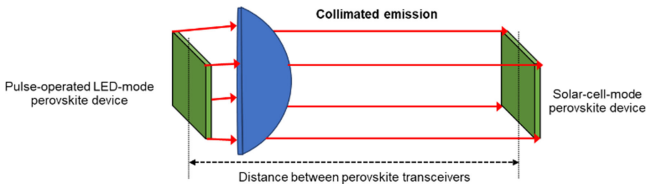

Fig. 11. System setup in Scenario 4.

lens is now put in between the perovskite optical transmitter and receiver. More specifically, this collimating lens is put just in front of the perovskite optical transmitter so that the light beam coming out from the lens is collimated. The diameter and focal length of the lens used in this study are 25.4 and 16 mm, respectively.

Unlike Section III, we find here that experimental data do not match the existing theory introduced in Section II, i.e., they do not follow (1). Moreover, there is a trade-off on the system performance when using and not using a collimating lens. Particularly, a collimating lens is useful to enhance the OWPT when two perovskite transceivers are perfectly aligned, because the magnitude of the output signal is much higher than that without the lens. However, the employment of a collimating lens narrows down the sliding distance between perovskite transceivers, since the output signal is quickly vanished when the sliding distance is increased, in the presence of the lens.

A. Scenario 4: Perovskite Optical Transceivers are Precisely Aligned, a Lens Is Used

This scenario is set up similarly to Scenario 1, but a collimating lens is put in front of the perovskite optical transmitter to irradiate the collimated light beam to the perovskite optical receiver, as illustrated in Fig. 11.

Experimental results in this scenario are shown in Fig. 12(a)–(b). We can clearly see that system performance in this scenario is very different from that of Scenario 1, where the perovskite receiver output is no longer dependent linearly on the inverse of the squared distance between perovskite transceivers. There

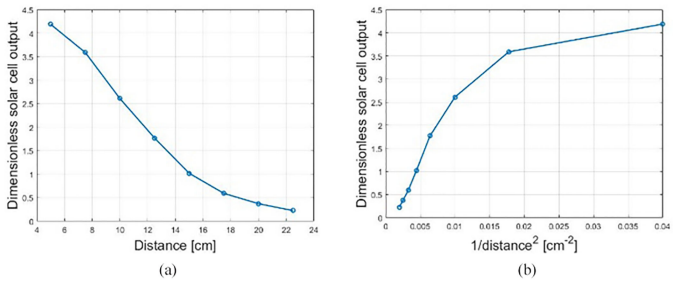

Fig. 12. System output versus inter-transceiver distance, when a collimating lens is used.

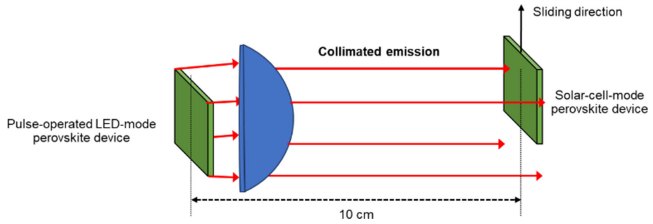

Fig. 13. System setup in Scenario 5.

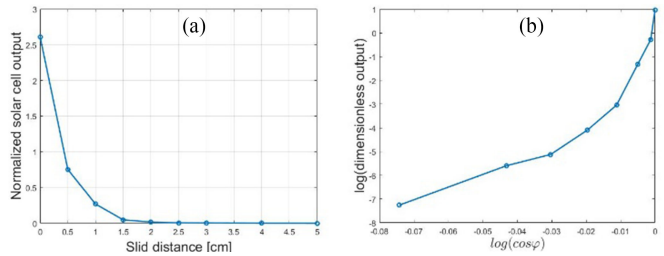

Fig. 14. System output versus inter-transceiver slid distance, when a collimating lens is used.

is no existing theory in the literature to be applicable to this scenario.

B. Scenario 5: Perovskite Optical Transceivers are Vertically Slid, a Lens Is Used

This scenario is only different from Scenario 2 that a collimating lens is employed to make the light beam from the perovskite optical transmitter collimated. The system setup is described in Fig. 13. Note that perovskite optical transmitters can also be slid in a different direction. However, such a case can be verified in a similar manner, and therefore we do not show here for conciseness.

The obtained results in Fig. 14(a) reveal that the perovskite optical receiver output is quickly decreased if the sliding distance between the transmitter and the receiver is increased, in the presence of a collimating lens. This can be explained as follows. When the sliding distance is increased, the angle of incidence φ and the angle of irradiance ϕ are bigger, hence the light intensity is much smaller, due to the term $\cos\varphi$. Moreover, a large portion of light emitted from the optical transmitter cannot reach the optical receiver because it is slid out of the range of the collimated beam. The combination of the above two reasons

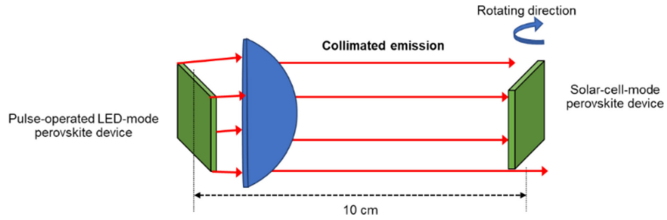

Fig. 15. System setup in Scenario 6.

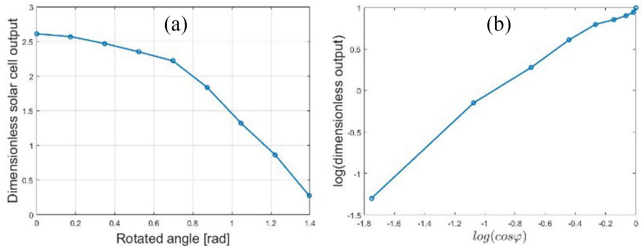

Fig. 16. System output versus optical receiver rotating angle, when a collimating lens is used.

results in the quick decay at the output of the optical receiver, as observed from the experimental data.

Similar to Scenario 2, we verify the relation between the log of the perovskite optical receiver output and the log of $\cos\varphi$. Such relation obtained by the experimental data is depicted in Fig. 14(b), revealing that it is strongly nonlinear, i.e., it is completely different from the theory. Hence, further theoretical analysis is needed to explain the obtained experimental data.

C. Scenario 6: Perovskite Optical Transceivers are Rotated, a Lens Is Used

This scenario is similar to Scenario 3, except that a collimating lens is used to make the light beam from the perovskite optical transmitter collimated, as depicted in Fig. 15.

The relation between the log of the perovskite optical receiver output and the log of $\cos\varphi$ is shown in Fig. 16(b) using the obtained experimental data. As can be observed in Fig. 16(b), such relation is not linear by the experimental data. Thus, a further theoretical study is required for an explanation of the obtained experimental data.

VI. Data-Driven Model for Perovskite-Based OWPT With a Collimating Lens

As seen in Section V, the existing theory described in Section III cannot be employed to explain the obtained experimental data when a collimating lens is used. Therefore, in this section, we aim at deriving a data-driven mathematical model to be fitted with experimental data. Interestingly, we find that the mathematical model shown in (4) can be utilized to be well fitted with all three scenarios presented in Section V, where $\boldsymbol{a}$, $\boldsymbol{b}$, $\boldsymbol{c}$, $\boldsymbol{d}$ are parameters of the model and $\boldsymbol{x}$ is the variable to which we want to fit the obtained data with.

$$\frac{ax^2 + bx + c}{x + d} \tag{4}$$

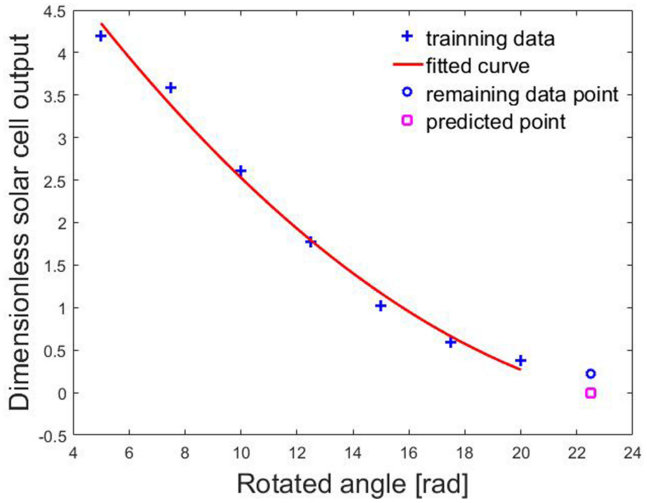

Fig. 17. Performance verification of the proposed data-driven model for Scenario 4.

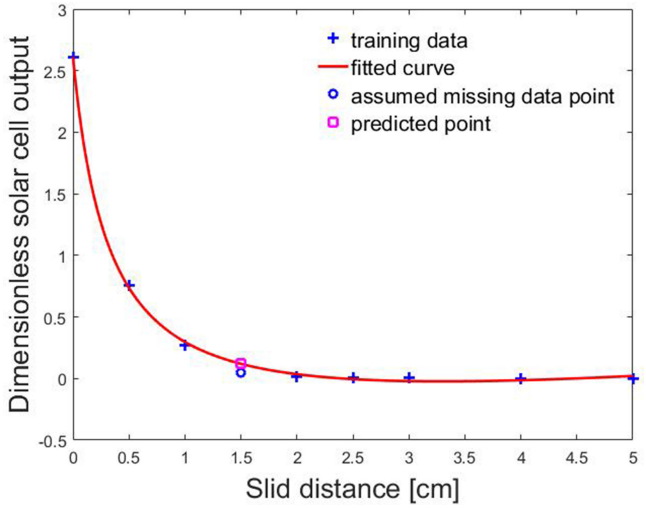

Fig. 18. Performance verification of the proposed data-driven model for Scenario 5.

The data-driven mathematical model in (4) has physical meanings. First, it contains a term describing the reverse dependence of the OWPT system on the considered variable (inter-transceiver distance, slid distance, or rotating angle). Second, the rational model in (4) also includes another term showing that the OWPT system output does not simply inversely depend on the considered variable.

Note that different data-driven models could be developed for each of Scenarios 4, 5, and 6, however we observe that none of them is applicable for all of these three scenarios. Hence, we only introduce here the analysis results with the model introduced in (4). Next, to verify the accuracy of the data-driven model in (4) on representing the dynamics of our considering perovskite-based OWPT, we perform additional tests as follows.

In Scenario 4, we use the first seven data points to train the data-driven model in (4), i.e., to determine its parameters. Consequently, the determined parameters are utilized to predict the dimensionless output of the perovskite optical receiver in accordance with the inter-transceiver distance of 22.5 cm. The fitted curve corresponding to the first seven data points as well as the predicted and realistic dimensionless output of the perovskite optical receiver are then shown in Fig. 17. It can be seen that the predicted output is quite close to the real one obtained from the experiment. Hence the proposed data-driven model in (4) works reasonably well.

With Scenario 5, we assume that one data point is missed or is not measured, while using the rest to train the data-driven model in (4). The trained model is then used to extrapolate or predict the dimensionless output of the perovskite optical receiver at the missed sliding distance (1.5 cm in this test). The fitted curve obtained from training data points, the predicted and assumed missing points are then shown in Fig. 18. We can observe that the predicted and assumed missing points are very close to each other, showing the good performance of the proposed data-driven model in (4).

Finally, in Scenario 6 we train the model in (4) in a similar manner as that for Scenario 4, where the first five data points are used for training and the last two data points are employed for verification. Then the fitted curve, the predicted and realistic dimensionless output of the perovskite optical receiver at two rotating angles are depicted in Fig. 19, showing the excellent performance of the trained model with predicted values almost identical with realistic ones.

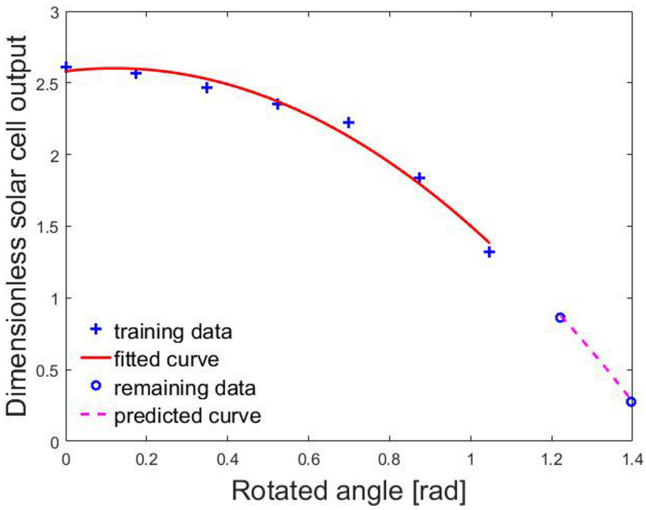

Fig. 19. Performance verification of the proposed data-driven model for Scenario 6.

VII. Conclusion

This paper presents the latest experimental results on optical wireless power transfer between two perovskite transceivers and their analysis to better illustrate the viability of the previously proposed thing-to-thing optical wireless power transfer concept. The experiments were performed under different settings to account for realistic situations, namely perfect and imperfect alignments between perovskite transceivers, where the perovskite optical receiver is slid and rotated in the latter context. Moreover,

a collimating lens is also used in both situations to verify its effects to the system operation.

Our experimental results indicate that if no collimating lens is employed, then the system performance is almost matched with the existing theory on the optical link DC gain computation for Lambertian-type LEDs, in both cases of perfect and imperfect alignments. Nevertheless, if a collimating lens is utilized to focus the lighting beam of the perovskite optical transmitter, then we found that the above-mentioned theory cannot be used to explain the obtained experimental results. Therefore, we empirically propose a data-driven mathematical model to be fitted with the obtained experimental data. Interestingly, we find that a mathematical model in the form of $\frac{ax^2+bx+c}{x+d}$ is usable for all scenarios when a collimating lens is used, where a, b, c, d are parameters of the model and x is the variable to which we want to fit the obtained data with. Additional tests are then performed to verify the above data-driven model in predicting the system output based on existing experimental data, showing its reasonable performance.

We also found that employing a collimating lens helps enhance the wireless power transfer in both magnitude and distance aspects, which is evidenced through the increased output of the perovskite optical receiver. However, there is a trade-off of tremendously reduced distance for wireless power transfer with a collimating lens when the perovskite transceivers are slid with each other. Thus, a careful consideration of using a collimating lens is needed in the realistic implementation of thing-to-thing wireless power transfer systems. For applications with stationary objects and a perfect alignment condition, a collimating lens should be utilized. On the other hand, for systems in which components can be moving, a collimating lens should not be used.

In the future research, a physics-driven model for the optical coupling link between optical transceivers made from perovskite solar cells, in the presence of a collimating lens or other lens should be developed. Moreover, additional experiments should be performed to obtain more data for validating the derived theoretical model. In another research line, the efficiency of perovskite optical transceivers in both light emission and absorption modes should be significantly improved in order to boost the efficiency of the whole OWPT system.

References

[1] Q. Zhang, W. Fang, Q. Liu, J. Wu, P. Xia, and L. Yang, "Distributed laser charging: A wireless power transfer approach," *IEEE Internet Things J.*, vol. 5, no. 5, pp. 3853–3864, Oct. 2018.

[2] W. Wang, Q. Zhang, H. Lin, M. Liu, X. Liang, and Q. Liu, "Wireless energy transmission channel modeling in resonant beam charging for IoT devices," *IEEE Internet Things J.*, vol. 6, no. 2, pp. 3976–3986, Apr. 2019.

[3] J. Fakidis, S. Videv, S. Kucera, H. Claussen, and H. Haas, "Indoor optical wireless power transfer to small cells at nighttime," *J. Lightw. Technol.*, vol. 34, no. 13, pp. 3236–3258, Jul. 2016.

[4] J. Kim *et al.*, "Active photonic wireless power transfer into live tissues," *Proc. Nat. Acad. Sci.*, vol. 117, no. 29, pp. 16856–16863, 2020.

[5] J. Jeong *et al.*, "An implantable optogenetic stimulator wirelessly powered by flexible photovoltaics with near-infrared (NIR) light," *Biosens. Bioelectron.*, vol. 180, 2021, Art. no. 113139.

[6] L. Sun, C. Cheng, S. Wang, J. Tang, R. Xie, and D. Wang, "Bioinspired, nanostructure-amplified, subcutaneous light harvesting to power implantable biomedical electronics," *ACS Nano*, vol. 15, pp. 12475–12482, 2021.

[7] D. H. Nguyen, T. Matsushima, C. Qin, and C. Adachi, "Towards thing-to-thing optical wireless power transfer: Metal halide perovskite transceiver as an enabler," *Front. Energy Res.*, vol. 9, 2021, Art. no. 679125. doi: 10.3389/fenrg.2021.679125.

[8] D. H. Nguyen, "Optical wireless power transfer for moving objects as a life-support technology," in *Proc. IEEE 2nd Glob. Conf. Life Sci. Technol.*, Mar. 2020, pp. 405–408.

[9] J. I. D. O. Filho, A. Trichili, B. S. Ooi, M. -S. Alouini, and K. N. Salama, "Toward self-powered internet of underwater things devices," *IEEE Commun. Mag*, vol. 58, no. 1, pp. 68–73, Jan. 2020.

[10] D. H. Nguyen and A. Chapman, "The potential contributions of universal and ubiquitous wireless power transfer systems toward sustainability," *Int. J. Sustain. Eng.*, vol. 14, no. 6, pp. 1780–1980, 2021. doi: 10.1080/19397038.2021.1988187.

[11] N. Kawashima and K. Takeda, "Laser energy transmission for a wireless energy supply to robots," in *Robotics and Automation in Construction*, C. Balaguer and M. Abderrahim, Eds. IntechOpen, [Online]. Available: https://www.intechopen.com/chapters/5576

[12] K. Jin and W. Zhou, "Wireless laser power transmission: A review of recent progress," *IEEE Trans. Power Electron.*, vol. 34, no. 4, pp. 3842–3859, Apr. 2019.

[13] P. D. Diamantoulakis, G. K. Karagiannidis, and Z. Ding, "Simultaneous lightwave information and power transfer (SLIPT)," *IEEE Trans. Green Commun. Netw.*, vol. 2, no. 3, pp. 764–773, Sep. 2018.

[14] A. W. S. Putra, M. Tanizawa, and T. Maruyama, "Optical wireless power transmission using Si photovoltaic through air, water, and skin," *IEEE Photon. Technol. Lett.*, vol. 31, no. 2, pp. 157–160, Jan. 2019.

[15] E. Moon *et al.*, "Bridging the 'Last millimeter' gap of brain-machine interfaces via near-infrared wireless power transfer and data communications," *ACS Photon.*, vol. 8, no. 5, pp. 1430–1438, 2021.

[16] A-H Lee, J. Lee, J. Jang, A. Nurmikko, and Y-K Song, "Wireless addressable cortical microstimulators powered by near-infrared harvesting," *ACS Sensors*, vol. 6, no. 7, pp. 2728–2737, 2021.

[17] D. Dregely, K. Lindfors, M. Lippitz, N. Engheta, M. Totzeck, and H. Giessen, "Imaging and steering an optical wireless nanoantenna link," *Nat. Commun.*, vol. 5, 2014, Art. no. 4354.

[18] J. Tang, K. Matsunaga, and T. Miyamoto, "Numerical analysis of power generation characteristics in beam irradiation control of indoor OWPT system," *Opt. Rev.*, vol. 27, pp. 170–176, 2020.

[19] M. Liu *et al.*, "Simultaneous mobile information and power transfer by resonant beam," *IEEE Trans. Signal Process.*, vol. 69, pp. 2766–2778, 2021.

[20] G. Tumen-Ulzii, A. Morgan, T. Matsushima, and C. Adachi, "Unintentional passivation of 4-tertbutyl pyridine for improved efficiency and decreased operational stability of perovskite solar cells," *Appl. Phys. Lett.*, vol. 118, no. 24, 2021, Art. no. 241603.

[21] G. Tumen-Ulzii *et al.*, "Understanding the degradation of spiro-ometad-based perovskite solar cells at high temperature," *J. Phys. Mater.*, vol. 4, no. 10, 2020, Art. no. 2000305.

[22] Q. Ding, L. Lei, J. Mendes, and F. So, "Operational stability of perovskite light emitting diodes," *Sol. RRL*, vol. 3, no. 1, 2020, Art. no. 012002.

[23] S. Watanabe, T. Cheng, G. Tumen-Ulzii, C. Qin, T. Matsushima, and C. Adachi, "Excited-state stability of quasi-two-dimensional metal halide perovskite films under optical and electrical excitations," *Appl. Phys. Lett.*, vol. 115, no. 23, 2019, Art. no. 233502.

[24] T. Cheng, G. Tumen-Ulzii, D. Klotz, S. Watanabe, T. Matsushima, and C. Adachi, "Ion migration-induced degradation and efficiency roll-off in quasi-2D perovskite light-emitting diodes," *ACS Appl. Mater. Interfaces*, vol. 12, no. 29, pp. 33004–33013, 2020.

[25] S. Shao *et al.*, "Elimination of the light soaking effect and performance enhancement in perovskite solar cells using a fullerene derivative," *Energy Environ. Sci.*, vol. 9, no. 7, pp. 2444–2452, 2016.

[26] T. Du *et al.*, "Light-intensity and thickness dependent efficiency of planar perovskite solar cells: Charge recombination versus extraction," *J. Mater. Chem. C*, vol. 8, no. 36, pp. 12648–12655, 2020.

[27] T. S. Sherkar *et al.*, "Recombination in perovskite solar cells: Significance of grain boundaries, interface traps, and defect ions," *ACS Energy Lett.*, vol. 2, no. 5, pp. 1214–1222, 2017.